SCIENTIFIC REPORTS

OPEN

SUBJECT AREAS:
TWO-DIMENSIONAL MATERIALS
SYNTHESIS OF GRAPHENE
ELECTRONIC MATERIALS
ELECTRONIC DEVICES

Received
23 April 2013

Accepted
27 August 2013

Published
11 September 2013

Correspondence and requests for materials should be addressed to L.W. (lmwei@sjtu.edu.cn); Y.Z. (yfzhang@sjtu.edu.cn) or W.Y. (pharmacy_ywe@126.com)

# Spontaneous intercalation of long-chain alkyl ammonium into edge-selectively oxidized graphite to efficiently produce high-quality graphene

Liangming Wei[1], Fei Wu[2], Diwen Shi[1], Changchen Hu[1], Xiaolin Li[1], Weien Yuan[2], Jian Wang[1], Jiang Zhao[1], Huijuan Geng[1], Hao Wei[1], Ying Wang[1], Nantao Hu[1] & Yafei Zhang[1]

[1]Key Laboratory for Thin Film and Microfabrication of the Ministry of Education, Institute of Micro/Nano Science and Technology, Shanghai Jiao Tong University, Shanghai, 200240, P. R. China, [2]School of Pharmacy, Shanghai Jiao Tong University, Shanghai 200240, China.

**Mass production of high-quality graphene nanosheets (GNs) is essential for practical applications. We report that oxidation of graphite by low concentration $KMnO_4$ at relatively high temperature (60°C) leads to edge-selectively oxidized graphite (EOG) which preserves the high crystalline graphitic structure on its basal planes while the edges are functionalized by oxygen-containing groups. Long-chain tetradecyl-ammonium salt ($C_{14}N^+$) could be spontaneously intercalated into EOG to form intercalated EOG-$C_{14}N^+$ compounds. Gentle and short-time sonication of EOG-$C_{14}N^+$ in toluene can full exfoliate EOG into edge-oxidized graphene nanosheets (EOGNs) with concentration of 0.67 mg/ml, monolayer population up to 90% and lateral size from 1 μm to >100 μm. The EOG and EOGN films show excellent electrical conductance, which is far superior to their graphene oxide (GO) counterparts. Our method provides an efficient way to produce high-quality GNs, and the resultant EOG also can be directly used for production of multifunctional materials and devices.**

Graphene nanosheets (GNs), the first two-dimensional atomic crystal, have received tremendous interest in recent years due to its unique properties[1–7]. The practical application of GNs will require developing a method for mass preparation of this material. Several methods, including micromechanical cleavage by Scotch tape[5], chemical vapor deposition (CVD)[6–10], epitaxial growth on SiC[11–15], and liquid-phase exfoliation of graphite[16–23], have been developed to produce GNs. The micromechanical cleavage method gives the highest-quality GNs, but it is unsuitable for mass preparation of this intriguing material. On the other hand, GNs can be grown on SiC wafer by sublimating Si from SiC. However, epitaxial growth on SiC suffers from two major disadvantages: the high cost of the SiC wafer and the high temperature used (>1000°C), which are not directly compatible with silicon electronics technology[1]. Large-area GN films have been prepared by CVD[6–10], but at present, the CVD process is expensive for mass production owing to requiring extremely careful fabrication and large energy consumption[1].

Liquid-phase exfoliation of graphite allows large-scale production of GNs via an all-solution process[16–23]. High-quality GNs have been prepared by exfoliation of pristine graphite in solvent N-methyl-pyrrolidone (NMP)[16], but the concentration of GN dispersions is low (~0.01 mg/ml), making many application impractical. Alternatively, GNs can be prepared from the graphite in water or organic solvent with surfactant or polymer coating[18–23]. To full exfoliate the graphite into GNs and stabilize the GN suspension with surfactants or polymers, harsh or long time sonication is always necessary, which leads to destruction of GNs (most of GNs having a lateral size less than 1 μm)[18–23]. Exfoliation of graphite intercalated compounds (GIC) has also been considered as an efficient way to produce GNs. However, so far, these GIC exfoliation methods still produce GNs with low monolayer population or small lateral sizes[24,25].

Extensive researches have been carried out to exfoliate graphite into graphene oxide (GO) by harsh oxidation, followed by reduction of GO back to the parent graphene state[26–31]. GO is chemically functionalized by oxygen-containing groups on both basal planes and edges, and has larger interlayer distance than parent graphite (~8Å vs. 3.35 Å), which makes GO easy to be completely exfoliated into single nanosheets in water or other polar

organic solvent. But the electrical properties of GO are severely damaged by harsh oxidation. In fact, GO is an insulator, which is significantly different from the semi-metallic graphenes[19]. Although reduction can partially recover the conductivity, considerable structural defects still exist on the reduced GO[32,33], compromising some of the unique properties and morphology of the pristine graphene[18].

More recently, In-Yup Jeon et al. have reported a method for edge-selectively carboxylated functionalization of graphite (ECG) without the basal plane oxidation by ball milling in the presence of dry ice[34]. Because ECG preserves the high crystalline graphitic structure on its basal plane, its electrical conductance is superior to its GO counterparts. This ECG sample could be exfoliated into GNs with monolayer population of about 25% in polar solvent, but ball milling also significantly breaks the large GN flake into small pieces.

Here, we reported that oxidation of graphite by low concentration $KMnO_4$ at relatively higher temperature (60°C) (the most common Hummers method used for preparation of GO is performed under lower than 40°C)[35] could lead to edge-selectively oxidized graphite (EOG) with low degree oxidation (Figure 1). More importantly, we observed long-chain tetradecyl-ammonium salt ($C_{14}N^+$) could be spontaneously intercalated into EOG to form intercalated EOG-$C_{14}N^+$ compounds. Only mild sonication of EOG-$C_{14}N^+$ for short time in nonpolar solvent can full exfoliate EOG-$C_{14}N^+$ into edge-oxidized graphene nanosheets (EOGNs) with concentration of 0.67 mg/ml and monolayer population up to 90%. In addition, most of EOGNs show large flake size from 1 μm to >100 μm. Finally, EOG films show excellent electrical conductance even if they are not deoxidized, which is far superior to their GO counterparts.

## Results

**Synthesis and characterization of EOG.** Hummers method is generally used to prepare GO[26,35]. Such method involves harsh oxidation of graphite in the presence of high concentrated $KMnO_4$ (generally, the mass ratio of $KMnO_4$/graphite >3) and sulfuric acid. Although $KMnO_4$ is generally used as oxidant, the active species in Hummers method is diamanganese heptoxide ($Mn_2O_7$), which is formed by the reaction of $KMnO_4$ with sulfuric acid[30]. $Mn_2O_7$ is far more reactive than its monometallic tetraoxide counterpart, but it can decompose into less oxidizing production ($MnO_2$, $O_2$) when heated to temperatures higher than 55°C[30,36] (the reaction shown below). So, for preparation of GO using Hummers method, the temperature needs to be kept low (less than 40°C).

$$KMnO_4 + 3H_2SO_4 \rightarrow K^+ + MnO_3{}^+ + H_3O^+ + 3HSO_{4-} \quad (1)$$

$$MnO_3^+ + MnO_{4-} \rightarrow Mn_2O_7 \quad (2)$$

$$2Mn_2O_7 \rightarrow 4MnO_2 + 3O_2 \ (T > 55^oC) \quad (3)$$

Here we prepared EOG by a method somewhat like Hummers method, but 5 times lower concentration of $KMnO_4$ together with high temperature oxidation (60°C) was used. In this reaction system, several types of oxidizers might exist ($MnO_3{}^+$, $MnO_4{}^-$, $Mn_2O_7$ and $MnO_2$) at the early stage of the oxidation reaction. The edges of graphite were first oxidized by these oxidizers (it is well-known the edge carbon atoms are more reactive than those at the basal planes, and oxidation start preferentially at edge planes[37,38]), but further oxidization of the little chemical reactive basal planes was suppressed because large numbers of strong oxidizers ($Mn_2O_7$) were decomposed into less oxidizing $MnO_2$ as the reaction proceeds. Elemental analyses show that EOG has lower oxygen content than Hummers GO (15% vs. ~50%), suggesting a low degree oxidation for EOG. Field emission scanning electron microscopy (FE-SEM) images show a compact edge surface for pristine graphite particles (Figure 2A), while a loose and expanded edge surface was observed in EOG sample (Figure 2B). We also fabricated EOG paper by vacuum filtration of EOG suspension. FE-SEM image reveals that the fracture edges of EOG paper exhibit a turbostratic structure (Figure 2C), which is different from the highly ordered layered structure for reduced GO paper prepared using same method[39]. These results suggest the oxygen-containing groups on the edges might distort and expand the edge structure. We performed Fourier transform infrared (FTIR) spectroscopic measurement to insight the chemical structures of the graphite, EOG and GO samples (Figure 2D). All samples show two absorption bands at around 3400 and 1032 $cm^{-1}$ attributable to absorbed water molecules and structural C-O groups. Both EOG and GO exhibit a band at 1725 $cm^{-1}$, which is assigned to C=O groups. This band is pronounced in GO sample due to higher degree oxidation. ECG gives a strong peak at 1230 $cm^{-1}$ exclusively from the C–O stretching in carboxylic acid (O=C-OH) groups[34], whereas GO shows board C-O stretching bands from 1000 to 1400 $cm^{-1}$, indicating coexistence of O=C-OH (carboxyl), C-O-C (epoxy), and C-OH (hydroxyl)[40,41]. It is well-known that epoxy and hydroxyl groups are bound on both edges and basal planes while carboxyl groups are mainly grafted on the edges of the oxidized graphite[34,40,41]. This suggests the edge-carboxylation of EOG. Pristine graphite and EOG display a sharp band centered at 1575 $cm^{-1}$ which has been assigned to the stretching of C=C bonds[41]. This band disappeared in GO, and instead a band at 1624 $cm^{-1}$, assigned to absorbed water[40,41], was observed. This result is consistent with the fact that EOG remains π-conjugated structure due to few (or no) basal plane oxidations, while the $sp^2$-bonded basal planes in GO are severely damaged by the oxygen-containing groups and other structural defects.

The samples were further characterized by powder X-ray diffraction (XRD) (Figure 2E). XRD patterns show a strong and sharp [002] peak at 26.5° for the pristine graphite, corresponding to an ideal layered-structure with d-spacing of 0.335 nm[42]. This [002] peak was significantly shifted from 26.5° to 10.8°, corresponding to an interlayer distance increase from 0.335 to 0.818 nm for GO. This large increase in the interlayer distance is due to the uptake of a water monolayer between the hydrophilic interlayer space of GO whose

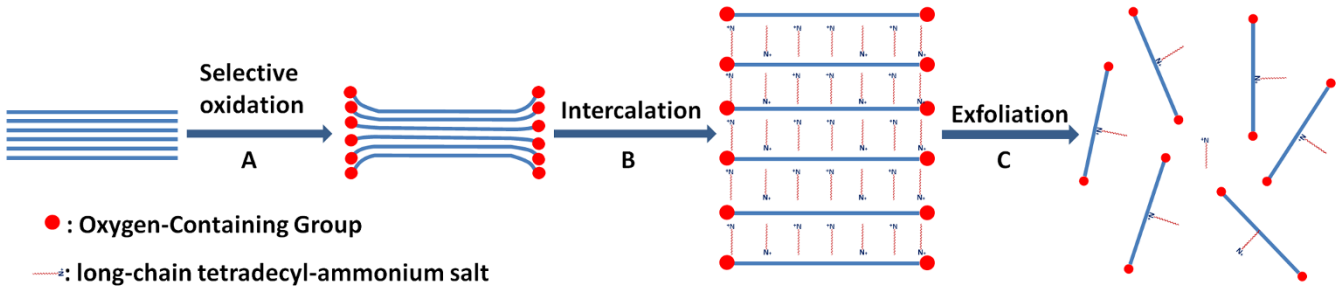


**Figure 1 | Schematic illustration for the preparation of monolayer graphene.** (A) Edge-selective oxidization of graphite (EOG) by low concentration of $KMnO_4$ at 60°C. (B): Long-chain tetradecyl-ammonium salt ($C_{14}N^+$) spontaneous intercalated into EOG. (C) Gentle and short time sonication to exfoliate EOG into monolayer graphenes.

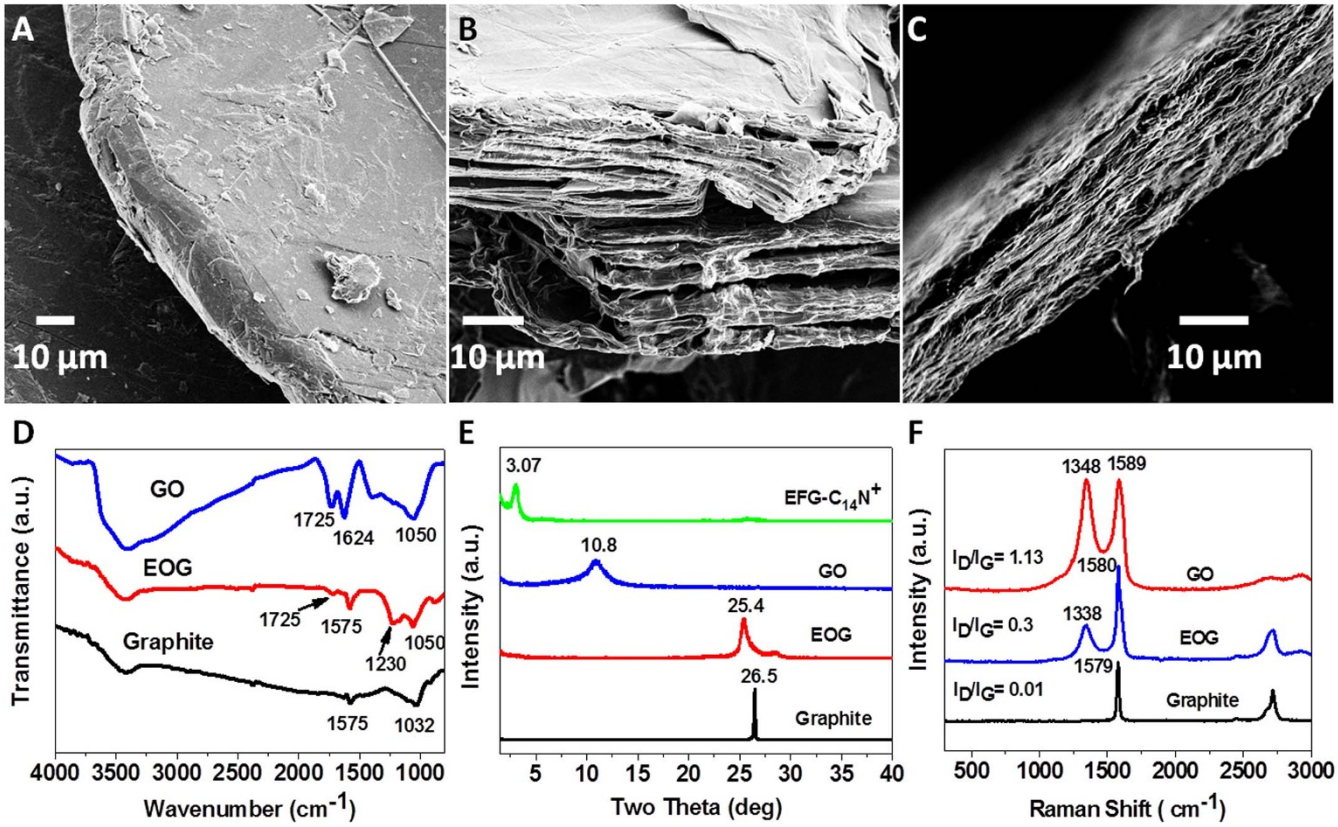


**Figure 2** | FE-SEM side-view images of pristine graphite (A), EOG (B) and EOG paper (C). (D) FTIR of pristine graphite, EOG and GO. (E) XRD of pristine graphite, EOG, GO and EOG-$C_{14}N^+$ intercalated compound. (F) Raman spectra of pristine graphite, EOG and GO.

basal planes are heavily oxidated[43]. The [002] peak becomes board, and slightly shifts from 26.5° to 25.4° for EOG samples, corresponding to an interlayer distance increase from 0.335 to 0.35 nm. This imperceptible increase in the interlayer distance suggests most of oxygen-containing groups are not introduced onto the basal planes of EOG but grafted onto the edges of graphite. The edge-selective functionalization of graphite could lead to an edge-expansion in solid state, which was confirmed by the board [002] peak of EOG[34]. In a control experiment, graphite was oxidized at 20°C. We observed that the resultant sample was a mixture of GO and graphite, as evidenced by two distinct [002] peaks at 11.2° and 26.3° (see Figure S1). This result indicates that high temperature oxidation (60°C) is necessary to obtain pure EOG.

The EOG sample was further characterized by Raman spectroscopic measurement. As seen in Figure 2F, the sharp and strong G (~1580 $cm^{-1}$) bands are clearly observed in both pristine graphite and EOG samples. The D band (1338 $cm^{-1}$) associated with the edge distortion and structural effects[44] is hardly visible in the pristine graphite. But GO shows a strong and broad D band with a ratio of the D band to G band intensity ($I_D/I_G$) to be about 1.13 due to edge effect and presence of large number of chemical and structural defects on both edges and basal planes. In contrast, EOG shows a D band with $I_D/I_G$ = ~0.3. This D band could be attributed to edge distortion by introducing chemical defects on the edges. To confirm the edge-selective oxidation, micro-Raman spectra were recorded at the edges and on the basal planes of graphite, GO and EOG sheets (Figure 3). As expected, pristine graphite shows very week D bands ($I_D/I_G \leq 0.1$) at both edge and basal planes (Figure 3A), whereas GO exhibits broad and strong D bands ($I_D/I_G \geq 1.1$) at both edge and basal planes (Figure 3B). In contrast, EOG shows a much higher $I_D/I_G$ ratio at the edge ($I_D/I_G = 1$) than the corresponding value ($I_D/I_G = 0.25$) on the basal planes (Figure 3C). These results further confirm the edge-selective oxidation of graphite in EOG samples. After EOG was thermally annealed at 800°C, the D band intensity significantly decreased and the $I_D/I_G$ ratio is approximate to the value of the pristine graphite (Figure 3D), indicating the edge groups and structural defects within EOG could be removed by thermal annealing.

The X-ray photoelectron spectra (XPS) spectroscopic measurement also confirmed the edge-selective oxidation. As shown in Figure 4A, the pristine graphite exhibits a pronounced C1s peak (~284.5 eV) and a weak O1s peak (~532 eV) arising from the physically adsorbed oxygen[34,45]. An increase in the ratio of O1s peak intensity relative to the C1s peak was observed in GO and EOG samples, indicating GO and EOG contain more oxygen-containing groups than pristine graphite (Figure 4A). High resolution XPS C1s peaks (Figure 4B) show that besides the C1s peak at 284.8 eV, a higher binding energy (287 eV) corresponding to C-O species was observed in GO and EOG samples. As expected, GO contained more C-O species than EOG. These C-O species were removed by 800°C annealing in Ar (Figure 4C). The annealed EOG exhibits the same C1s XPS spectrum as pristine graphite, confirming the lack of significant defects on the annealed EOG. In contrast, annealed GO sample shows broader C1s peak than pristine graphite, suggesting significant number of structural defects still exist on the annealed GO. Raman spectra (Figure 4D) show that the annealed EOG exhibits very weak D band, just like pristine graphite, but the annealed GO shows strong and broad D band associated with the edge distortion and presence of structure defects. XRD results (Figure 4E) also show that annealing of EOG restores the sharp [002] peak, corresponding to ideal layered structure, while annealed GO exhibits completely disordered structure, which might be ascribed to gas (evolving from intercalated water and functional groups) released from basal planes, leading to explosive expansion of GO[19,45]. For EOG sample, oxidation of graphite was relatively mild, and the covalently attached

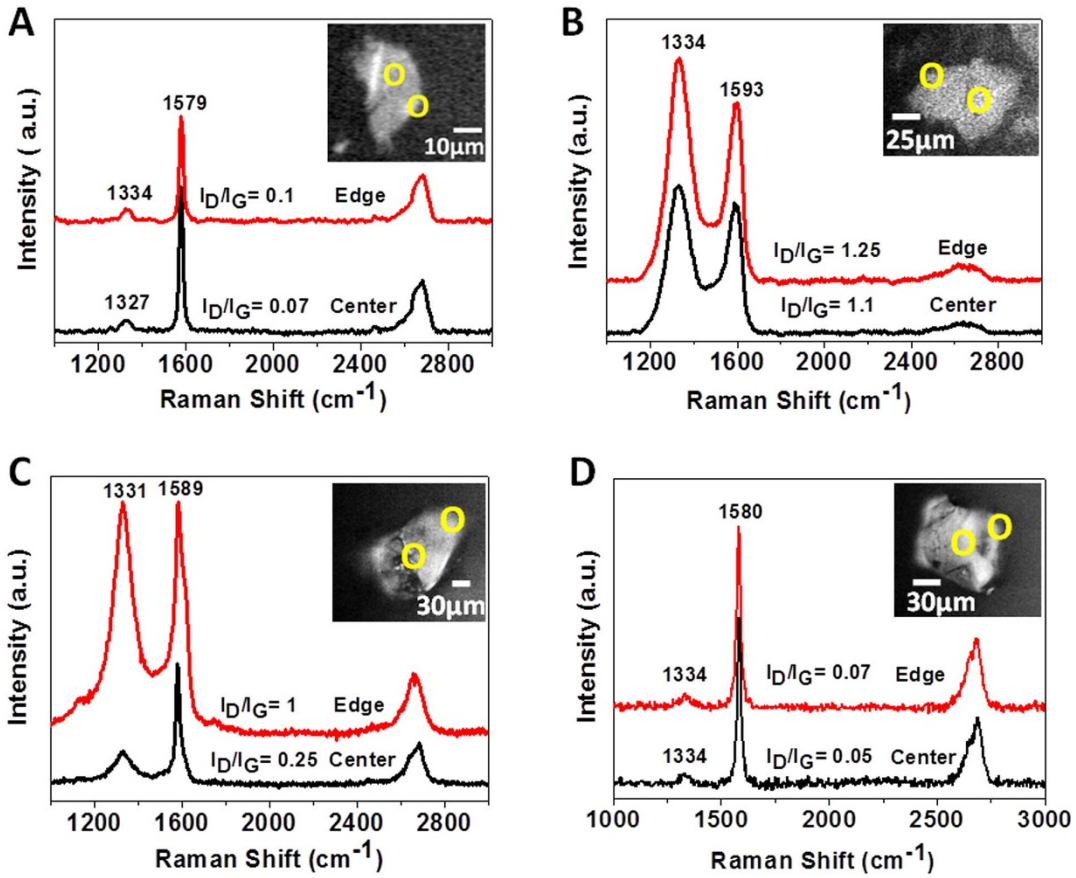


**Figure 3** | (A) Micro-Raman spectra measured at the edge and on the basal plane of pristine graphite (A), GO (B), EOG (C) and annealed EOG (D).

functional groups were most at the edges of EOG. These edge groups can be easily removed by thermal annealing, leading to restore the structure of pristine graphite. In contrast, both edge and basal planes of the Hummers GO were severely damaged by harsh oxidation. Thermal annealing can remove the oxygen-containing groups from the edges but was unable to completely repair the large number of chemical and topological defects formed within the basal planes of the Hummers GO sheets[19].

**Exfoliation of EOG into EOGNs in solvent.** Although oxygen-containing groups were introduced on the edges of graphite, the resultant EOG cannot be dispersed and exfoliated into EOGNs in water, even if long time sonication was used, suggesting a hydrophobic nature for EOG. This behavior is similar to the pristine graphite, but strong contrast to the hydrophilic GO which was easy to be completely exfoliated into single sheets in water due to presence of abundant functional groups within the basal planes. EOGNs can be dispersed in *N*-methyl-2-pyrrolidone (NMP) and *N*,*N*-dimethylformamide (DMF), but the concentration of EOGN dispersion is very low (<0.02 mg/ml) and long time sonication (>12 h) is required.

In order to obtain single-layer GNs with high yield, we intercalated EOG with long-chain tetradecyl-ammonium salt ($C_{14}N^+$) to expand the distance between graphite layers and weaken the van der Waals interaction between graphite layers. During this process, EOG was only soaked in $C_{14}N^+$ basic aqueous solution, no other avenues (such as sonication, heating et al.) required to facilitate the intercalation reaction. As seen from the XRD patterns in Figure 2E, the soaked EOG shows a sharp diffraction peak at 3.07°, corresponding to an interlayer spacing of 2.94 nm, which is much larger than the interlayer spacing of 0.35 nm for parent EOG sample. This large increase in the interlayer spacing of EOG is consistent with intercalation of monolayer $C_{14}N^+$ (chain length: ~2nm) within the interlayer space of EOG (Figure 1). Gravimetric analysis indicated the EOG-$C_{14}N^+$ sample contained about 35% (w/w) $C_{14}N^+$. It should be mentioned that the large increase in the interlayer spacing is not due to the intercalation of solvent molecules (water) because no increase in the interlayer spacing was observed when soaking EOG without $C_{14}N^+$ (Figure S2). We also observed $C_{14}N^+$ cannot be intercalated in the pristine graphite (Figure S3). Introduction of oxygen-containing groups on the edges of graphite is the key for intercalation of $C_{14}N^+$ in the graphite. This intercalation reaction is sensitive to the size of the ammonium salt. When tetradecyltrimethylammonium salt ($C_{14}$ $N^+(CH_3)_3$) instead of $C_{14}N^+$ was used, large number of EOG was not intercalated with $C_{14}$ $N^+(CH_3)_3$, as evidenced by a strong [002] peak ascribed to parent EOG remaining in the resultant sample (Figure S4). It seems that the intercalation reaction was blocked by three methyl groups in $C_{14}$ $N^+(CH_3)_3$ due to steric effect.

The intercalated EOG-$C_{14}N^+$ compounds were readily dispersed and form a homogeneous black dispersion in benzene or toluene by low power bath sonication (100 W) for 30 min (Figure 5A). This dispersion was stable and no precipitation was observed after standing for three months. However, EOG-$C_{14}N^+$ cannot form a homogeneous and stable suspension in some polar solvents (water, ethanol, dimethyl sulfoxide (DMSO), DMF and NMP) by sonication under same condition, and they precipitated immediately from the suspension after stopping sonication. This result further confirmed the hydrophobic nature for EOGNs due to the weak oxidation and less destruction during sonication. Among all the solvents tested, toluene was found to be the best for dispersing EOG into a stable suspension, with the concentration of EOGNs in toluene up to 0.67 mg/mL (>30 times than that of EOGNs in NMP).

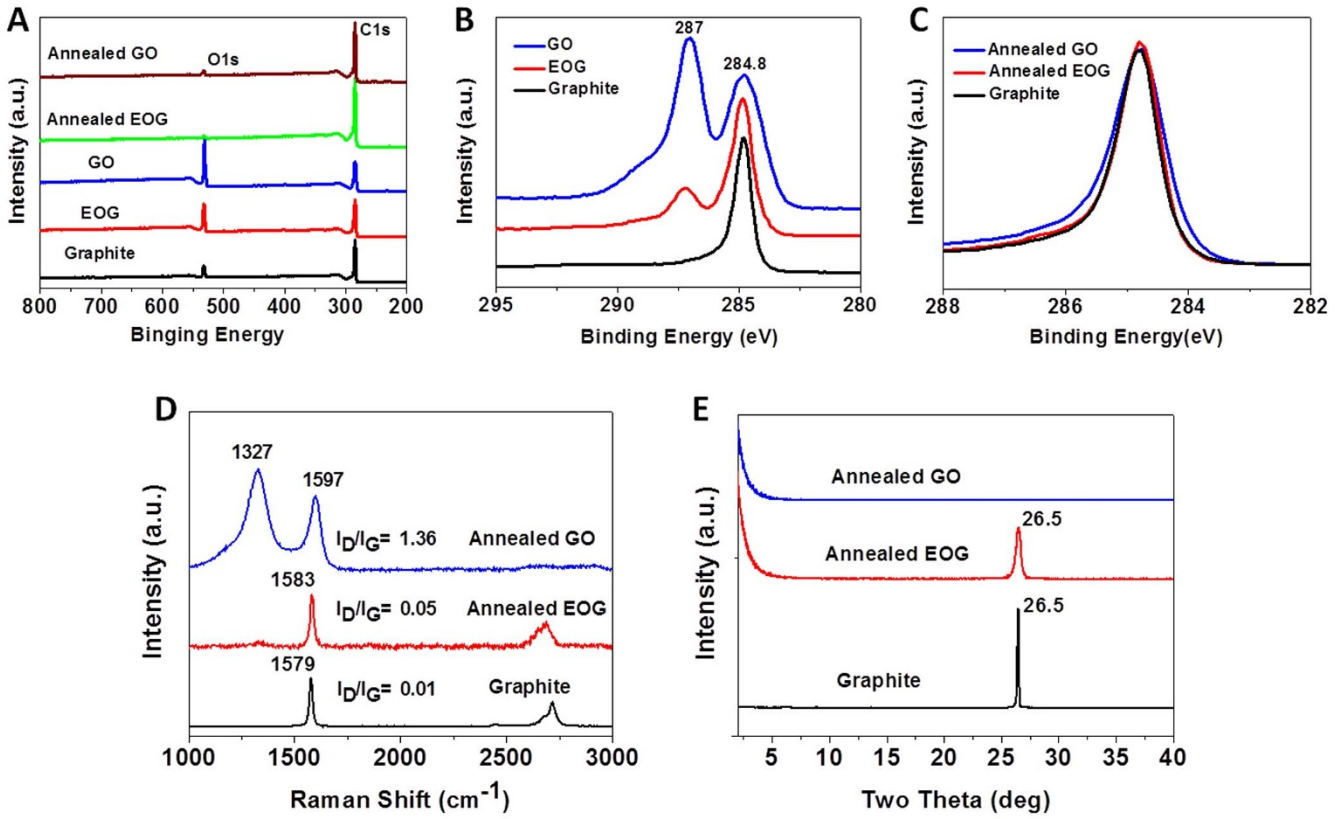


**Figure 4** | (A) XPS survey spectra of pristine graphite, EOG, GO, annealed EOG and annealed GO. (B) High resolution XPS C1s spectra of pristine graphite, EOG and GO. (C) High resolution XPS C1s spectra of graphite, annealed EOG and annealed GO. Raman spectra (D) and XRD patterns (E) of graphite, annealed EOG and annealed GO.

We used Atomic Force Microscopy (AFM) to characterize the EOG dispersion deposited on the cleaved mica surface (Figure 5B). For one hundred of exfoliated EOGNs measured, we observed that about 90% of EOGNs with average topographic height less than 1 nm are single-layer EOGNs with various shapes and sizes. The most of EOGNs have the lateral size larger than 1 μm, and very large EOGNs with size of >100 μm can also be observed. Transmission electron microscopy (TEM) and electron diffraction (ED) were also used to characterize the EOGNs (Figure 5C). The TEM shows the edges of EOGN have a tendency to "restack" with basal planes due to the strong van der Waals interactions between the defect-free basal planes and the oxidized edges. The ED pattern of the deposited EOGNs shows a typical sixfold symmetry peaks with the (0–100) spots appeared to be more intense relative to the (1–210) spots ($I_{0-100}/I_{1-210} > 1.5$), reflecting single layer of graphene with high crystallinity[46]. The above results clearly indicated that the intercalated EOG-$C_{14}N^+$ compounds were readily exfoliated into single layer EOGNs by mild sonication.

**Performance of EOG and EOGN film.** To demonstrate the functionality of the EOG flakes in the electronic applications, the electrical properties of EOG films was studied. A large scale EOG casted film was first prepared from EOG water suspension (Figure 6A). This casted film had an electrical resistance of 23.9 Ω when measured with hand-held multimeter (Figure 6B), which is a little higher than that of pristine graphite (<10 Ω)[46], but significantly lower than that of GO (>2 MΩ). The casted EOG film was further compressed by hydraulic press at 45 MPa to form EOG film with thickness of ~35 μm. The compressed EOG film had an electrical resistance of 0.51 Ω/□ measured with a four point probe, which is far superior to the insulating GO counterpart. Upon thermal annealed at 800°C for 2 h under argon to remove the edge groups on EOG, the EOG film shows electrical resistance of 0.15 Ω/□ while remains a cohesive film (Figure 6C). In contrast, thermal annealing a GO thin film led to an explosive expansion of GO film (intercalated water and functional groups might evolve into gas)[45], leaving few GO on the substrate surface (Figure 6C). As mentioned before, the annealed EOG retained ideal layered structure with less edge distortion and few (or no) structure defects within the basal planes, which is similar to the pristine graphite. Therefore, EOG is a better candidate than GO for the direct formation of cohesive and conductive GN films by high pressure compressing and subsequent thermal annealing.

We also used the EOGN dispersions in toluene to prepare transparent conductive films as shown in Figure 6D. This film was prepared by vacuum filtration of EOGN dispersions onto mixed cellulose ester membrane, transferred to a silica slice by dissolving away the ester membrane in acetone and thermal treatment at 800°C to remove the edge groups. The transparence (transparence defined as transmittance at wavelength of 550 nm) of the annealed EOG films varied from 13.8% to 81.8%, depending on the calculated thickness[9,47] (Figure 6E). Figure 6F illustrates the transparence-dependence of the sheet resistance, which shows that the sheet resistances of GN films are proportional to their transparencies. With the transparence varying from 13.8% to 82%, the sheet resistances increased from 170 Ω/□ to 26 KΩ/□, clearly showing that the conductivity of the annealed EOG thin films are superb to their GO counterparts (approximately 100 kΩ/□)[29,34] by a few orders of magnitude.

## Discussion

Intercalation of bulky organic molecules into interlayer of graphite to open the basal spacing and weaken the π-π interaction between graphite layers is a promising method to produce scalable and high quality graphene[19,48]. But the ~2 nm chain length of $C_{14}N^+$ suggests

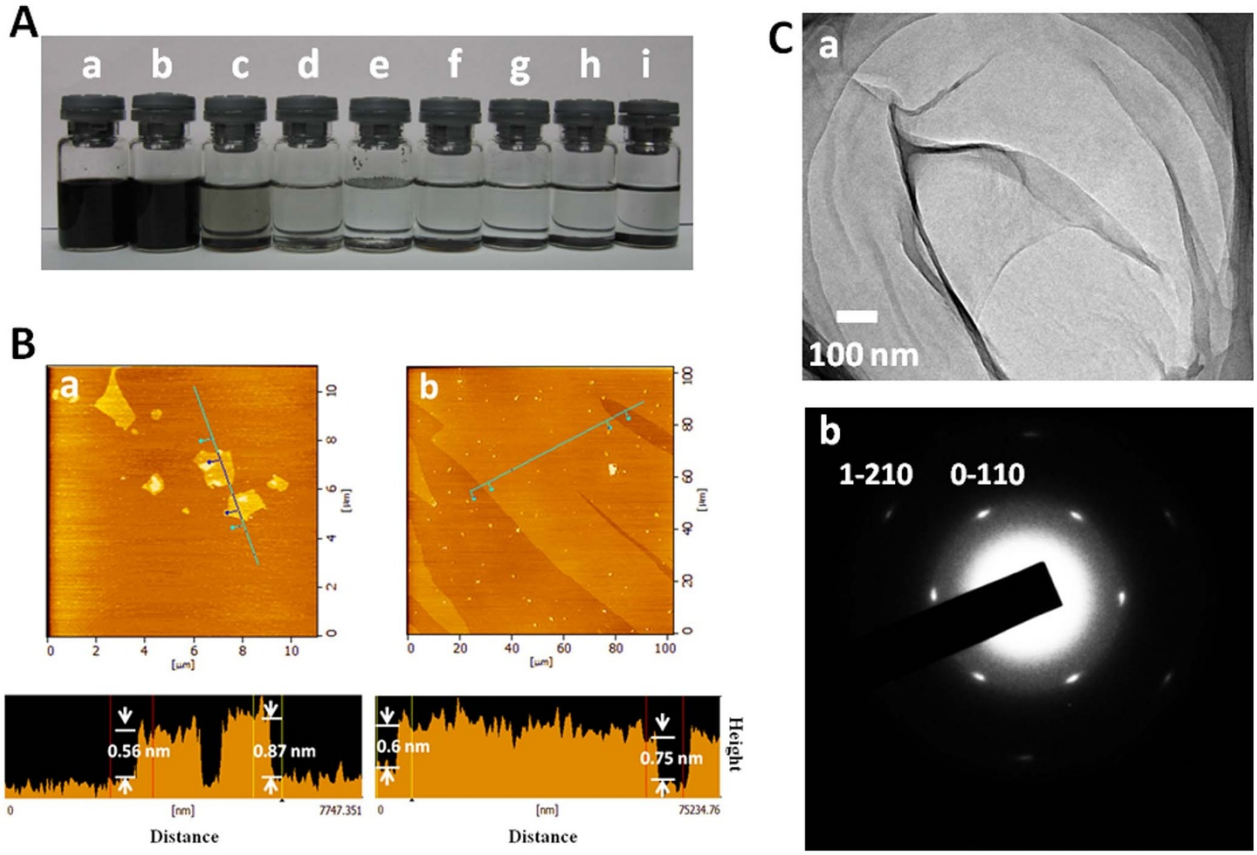


**Figure 5** | (A) Photographs of EOG dispersion after sonication of EOG-$C_{14}N^+$ in toluene (a), benzene (b), NMP (c), DMF (d), DMSO (e), ethanol (f), methanol (g), water (h) and acetone (i) for 30 min. The dispersions stand for 3 h after sonication. (B) AFM images of EOG nanosheets (EOGN) with different sizes deposited on mica. All samples show a topographic height of less than 1 nm. (C) TEM image of EOGN (a) and the corresponding electron diffraction (b).

this molecule is too large to intercalate and overcome the 0.335 nm basal spacing of the graphite planes. Indeed, no interaction reaction was observed when soaking pristine graphite in $C_{14}N^+$ solution, even if short chain molecules such as $C_{10}N^+$ were used (Figure S5). In the case of EOG, the spontaneous intercalation of $C_{14}N^+$ into the interlayer of EOG is definitely ascribed to the edge oxygen-containing groups. We expected that the edge functional groups (C-OH and COOH) on EOG could be dissociated into C-$O^-$ and $COO^-$ in the basic aqueous solution. The long chain $C_{14}N^+$ can be absorbed and intercalated into the edge planes of EOG via cation-anion interaction[49,50], resulting in large expansion of the edge surface of EOG and also switching the edges wettability from hydrophilic to hydrophobic. This facilitates further co-intercalation of $C_{14}N^+$ into the interlayer spaces of EOG via hydrophobic interaction (van der Waals interaction) between alkyl groups. Lagaly and Weiss[51] have systematically studied the hydrophobic interaction between alkyl groups in the layered materials and found that enthalpy change during absorption of alcohols into dodecylammonium-intercalated layered silicates increased with increase of alkyl chain length of alcohols (0.12–0.17 kJ/mol $-CH_2-$). For the case of $C_{14}N^+$, the hydrophobic interaction between long $C_{14}$ chains is sufficient for them to be co-intercalated and stay in the interlayer of EOG, leading to the large expansion of interlayer spacing.

EOG retained high crystallinity of the graphitic structure on its basal planes while its edge planes were functionalized by plenty of oxygen-containing groups. This featured structure makes EOG promising materials for advanced application. For example, we found that when EOG was used as electrode materials in lithium ion batteries, it exhibited much higher reversible capacity than reduced GO (340 vs. 220 mA h $g^{-1}$ at 40th cycle) (See Figure S6). This might be because that in EOG sample, lithium ion can be stored not only within the defect-free basal planes via intercalation reaction (just like in pristine graphite)[52], but also on the edge oxygen groups via Faradaic reaction between Li and oxygen ($C = O + Li^+ + e^- \leftrightarrow$ C-OLi)[53–56]. In contrast, the presence of large number of defects within the basal planes in reduced GO sample[19,34] could lead to more irreversible capacity. Additionally, for reduced GO sample, the lower oxygen coverage (10% vs. 15%) contributed less Faradaic capacity.

In summary, we have developed an efficient method for producing high-quality edge oxidized graphene nanosheets (EOGNs). It was first reported that long tetradecyl-ammonium salt ($C_{14}N^+$) could be spontaneously intercalated into edge-selectively oxidized graphite (EOG) to form intercalated EOG-$C_{14}N^+$compounds which could be full exfoliated into EOGNs in toluene by gentle and short time sonication. The resultant EOGNs are characterized by high monolayer population (90%), few defects on basal planes, relatively large lateral size and high concentration dispersion in non-polar solvent (0.67 mg/ml). A large area conductive EOG film could be prepared by a simple solution casting method. Since few defects exist on the basal planes of EOG, the electrical conductivity of EOG film is similar to that of pristine graphite, but significantly different from that of the insulating GO. Thermal annealing can readily remove the covalently linked edge groups from EOGNs and regenerate high-quality pristine GNs which exhibited many superior properties to its thermal-annealed GO counterparts. Additionally, while EOG is electrically conductive, the presence of reactive oxygen groups on the edges enables further chemical modification of EOG to form new type of

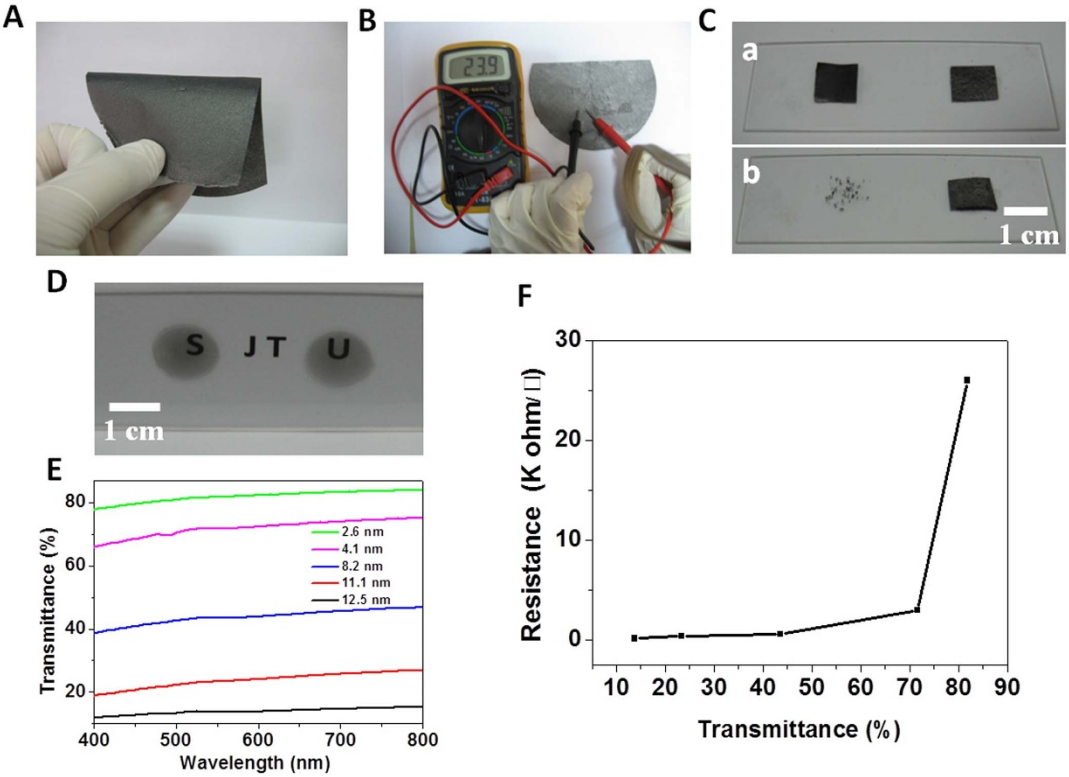


**Figure 6** | (A) Photographs of large EOG film. This film was prepared by pouring the EOG water suspension into a teflon mould, and then dried. (B) The electrical resistance of the EOG film measured with a hand-held multimeter. It shows an electrical resistance of 23.9 **Ω**. (C) Photographs of GO (left) and EOG (right) films before (a) and after (b) thermal annealing at 800°C. (D) Photographs of transparent EOGN films deposited on silica slice. These films were prepared by vacuum filtration of EOGN toluene dispersion onto mixed cellulose ester membrane, and then transferred to a silica slice by dissolving away the ester membrane in acetone. (E) Optical transmittance of EOGN film with calculated thickness. (F) Resistance of the EOGN films vs. the thermal-annealed EOGN transmittance at 550 nm.

chemically modified GNs, which could find a wide application in sensors, capacitors, batteries, electrocatalysts, and so on.

## Methods

**Edge-oxidized graphite (EOG) making.** In a typical synthesis of EOG, 1 g of natural graphite flakes (Sigma-Aldrich, Product Number 332461) were first ground with NaCl crystallites. NaCl was removed by water washing and vacuum filtration. The obtained graphite was then soaked in 23 ml of concentrated sulfuric acid. After the suspension was stirred for 12 h, 0.1 g of $NaNO_3$ and 0.7 g of $KMnO_4$ were added slowly for 1 h while the temperature was kept at 60°C (Caution: during adding $KMnO_4$, keep the container open and added slowly). The solution was then stirred for 2 days, and 3 ml of water was added. Another 3 ml of water was added after 5 minutes later, followed by 40 ml of water after 5 min. Another 140 ml of water and 10 ml of 30% $H_2O_2$ were added to end the reaction after 15 minutes. The suspension was then repeatedly centrifuged at 4500 rpm and washed with deionized water. The resultant EOG was dried at 80°C.

**Synthesis of tetradecylamine ammonium intercalated EOG (EOG-$C_{14}N^+$).** A 0.5 g of tetradecylamine was first dispersed in 20 ml of deionized water, and then the concentrated HCl solution was added into this suspension to transform tetradecylamine to tetradecyl-ammonium salt. The HCl was dropped until a transparent and weak basic (pH ≈ 9) tetradecyl-ammonium solution was obtained. Weighed 50 mg of EOG powder was then soaked in that tetradecyl-ammonium solution at 40°C for 4 days. After soaking, the suspension was filtered to remove un-intercalated tetradecyl-ammonium salt and $C_{14}N^+$-EOG was obtained. Last, the resultant EOG-$C_{14}N^+$ was air-dried.

**Exfoliation of EOGs to graphene.** The dried EOG -$C_{14}N^+$ was dispersed in 10 ml of toluene at a concentration of 1 mg/ml by ultrasonication in a low power sonic bath (100 W) for 30 minutes, and then centrifuged for 30 minutes at 400 rpm to remove any aggregates. After centrifugation, the top 1/2 homogeneous black dispersion was collected by pipet and retained for use.

*Graphite oxide (GO) synthesis.* GO was prepared by a modified Hummers method. Briefly, 5 g of graphite flakes was transferred to a 1000 mL round-bottom flask, and then 500 ml of concentrated sulfuric acid was added. The mixture was stirred at room temperature for 12 h and 3.7 g of $NaNO_3$ was added. Next, the flask was placed in an ice bath, and 16.8 g of $KMnO_4$ was slowly added to the flask for over 1 h. The suspension was stirred for 2 h in an ice bath and further stirred for 5 days at room temperature. Afterward, 20 mL of water was slowly added, followed by another 20 mL of water and 15 ml of $H_2O_2$ (30% aqueous solution). After the resultant mixture was diluted by 500 ml of water (slowly added), it was then centrifuged and washed with water for four times. The GO suspension was subjected to dialysis to remove residual salts and acids, and then dried at 80°C to form GO samples. To prepare reduced GO, the GO sample was mixed with hydrazine hydrate and stirred for 48 h at 40°C. This product was filtered and washed with distilled water and dried at 60°C under vacuum.

**Preparation of EOG or GO films.** EOG or GO film was prepared by pouring the EOG or GO suspension (in water) into a teflon mould, and then dried at 80°C for 24 h to form large EOG or GO film. These films can be further compressed at 45 MPa to produce films with diameter of 2 cm and thickness of about 30–40 μm. EOG film can also be prepared by filtration of EOG suspension through mixed cellulose ester membrane (200 nm pore size), followed by drying and peeling from the filter.

The EOGN thin films were also prepared from EOGN dispersion. This thin film was prepared by filtering approximately 3 mL of EOGN dispersion in toluene through mixed cellulose ester membrane having 200 nm average pore size. After the dispersion had passed through the membrane, the film was left to set over 30 minutes and then dried at 90°C for 12 h. This film was transferred to a silica slice by placing EOG film on the surface of a silica slice and then immersed in acetone to dissolve away the ester membrane. The film on the silica slices was dried at 80°C for 12 h, and then thermally annealed at 800°C for 2 h under Ar flow (100 ml/min) to remove the edge-on functional groups on EOG.

*Electrochemical experiments.* Half-cell tests were performed using CR2016-type coin cells with lithium-foil as counter electrode and EOG (or reduced GO) as working electrode, assembled in an argon-filled glove box with oxygen and water contents less than 10 ppm. The electrolyte was 1 M LiPF6 in the mixture of ethylene carbonate (EC) and dimethyl carbonate (DMC) (1 : 1 in volume ratio). The working electrode consisted of 80 wt% active material (EOG or reduced GO) and 20 wt% binder (polyvinylidene fluoride dissolved in N-methyl-2-pyrrolidone) which was mixed homogeneously and pasted on Cu foil. The electrochemical performances were tested

on a LAND battery test system (Wuhan Kingnuo Electronics Co., Ltd., China) at room temperature, in the voltage range of 0.01–3 V.

**Characterization.** The morphologies of the samples were observed by field emission scanning electron microscopy (FE-SEM, Carl Zeiss Ultra 55). Fourier transform infrared (FTIR) spectra were recorded on Perkin-Elmer 70 using KBr pieces. Powder X-ray diffraction (XRD) patterns were obtained with a RIGAKU diffractometer equipped with Cu Kα X-ray radiation, operated at 40 kV and 20 mA. The scattering and receiving slits were 1/6 and 0.3°, respectively. The transmission electron microscopy (TEM) images were obtained from JEOL 2100. TEM samples were prepared by sonication of EOG-$C_{14}N^+$ in toluene for 30 min and then evaporating a drop of sample solution onto carbon micro-grids. X-ray photoelectron spectra (XPS) were recorded on a Shimadzu/Kratos AXIS Ultra XPS spectrometer. Elemental analysis (EA) was conducted with Thermo Scientific Flash 2000. The Raman spectra were collected with a Dilor Labram-1B Raman spectrometer with He–Ne laser (633 nm) as the excitation source by using confocal Raman microscopy. Atomic Force Microscopy (AFM) images were obtained using an Environment Control Scanning Probe Microscope (SII Nanonavi E-Sweep). AFM sample was prepared by dropping EOG dispersion onto cleaved mica substrates and then dried at 80°C for 12 h to remove the solvent and absorbed water. The conductance of films was characterized by four point probe method using Four Probes TECH RST-8. The transparence of thin film samples on silica slices was measured by Lambda 950 UV/VIS/NIR spectrometer.


1. Novoselov, K. S. *et al.* A roadmap for graphene. *Nature* **490**, 192–200 (2012).
2. Geim, A. K. & Novoselov, K. S. The rise of graphene. *Nat. Mater.* **6**, 183–191 (2007).
3. Allen, M. J., Tung, V. C. & Kaner, R. B. Honeycomb carbon: a review of graphene. *Chem. Rev.* **110**, 132–145 (2010).
4. Georgakilas, V. *et al.* Functionalization of graphene: covalent and non-covalent approaches, derivatives and applications. *Chem. Rev.* **112**, 6156–6214 (2012).
5. Novoselov, K. S. *et al.* Electric field effect in atomically thin carbon films. *Science* **306**, 666–669 (2004).
6. Claussen, J. C. *et al.* Nanostructuring platinum nanoparticles on multilayered graphene petal nanosheets for electrochemical biosensing. *Adv .Funct. Mater.* **22**, 3399–3405 (2012).
7. Shang, N. G. *et al.* Catalyst-free efficient growth, orientation and biosensing properties of multilayer graphene nanoflake films with sharp edge planes. *Adv. Funct. Mater.* **22**, 3506–3514 (2008).
8. Li, X. S. *et al.* Large-area synthesis of high-quality and uniform graphene films on copper foils. *Science* **324**, 1312–1314 (2009).
9. Bae, S. K. *et al.* Roll-to-roll production of 30-inch graphene films for transparent electrodes. *Nat. Nanotechnol.* **5**, 574–578 (2010).
10. Mattevi, C., Kim, H. W. & Chhowalla, M. A review of chemical vapour deposition of graphene on copper. *J. Mater. Chem.* **21**, 3324–3334 (2011).
11. Taisuke, O., Bostwick, A., Seyller, T., Horn, K. & Rotenberg, E. Controlling the electronic structure of bilayer graphene. *Science* **313**, 951–954 (2006).
12. Virojanadara, C. *et al.* Homogeneous large-area graphene layer growth on 6*H*-SiC (0001). *Phys. Rev. B.* **78**, 245403(1)–245403(6) (2008).
13. Berger, C. *et al.* Electronic confinement and coherence in patterned epitaxial graphene. *Science* **312**, 1191–1196 (2006).
14. Strupinski, W. *et al.* Graphene epitaxy by chemical vapor deposition on SiC. *Nano Lett.* **11**, 1786–1791 (2011).
15. Lin, Y. M. *et al.* 100-GHz transistors from wafer-scale epitaxial graphene. *Science* **327**, 662 (2010).
16. Hernandez, Y. *et al.* High-yield production of graphene by liquid-phase exfoliation of graphene. *Nat. Nanotechnol.* **3**, 563–568 (2008).
17. Coleman, J. N. Liquid exfoliation of defect-free graphene. *Acc. Chem. Res.* **46**, 14–22 (2013).
18. Chabot, V., Kim, B., Sloper, B., Tzoganakis, C. & Yu, A. P. High yield production and purification of few layer graphene by gum Arabic assisted physical sonication. *Sci. Rep.* **3**, 1378 (2013).
19. Li, X. L. *et al.* Highly conducting graphene sheets and Langmuir-Blodgett films. *Nat. Nanotechnol.* **3**, 538–542 (2008).
20. An, X. H. *et al.* Stable aqueous dispersions of noncovalently functionalized graphene from graphite and their multifunctional high-performance applications. *Nano Lett.* **10**, 4295–4301 (2010).
21. Hamilton, C. E., Lomeda, J. R., Sun, Z. Z., Tour, J. M. & Barron, A. R. High-yield organic dispersions of unfunctionalized graphene. *Nano Lett.* **9**, 3460–3462 (2009).
22. Green, A. A. & Hersam, M. C. Solution phase production of graphene with controlled thickness via density differentiation. *Nano Lett.* **9**, 4031–4036 (2009).
23. Lotya, M., King, P. J., Khan, U., De, S. & Coleman, J. N. High-concentration, surfactant-stabilized graphene dispersions. *ACS Nano.* **4**, 3155–3162 (2010).
24. Geng, X. M. *et al.* Interlayer catalytic exfoliation realizing scalable production of large-size pristine few-layer graphene. *Sci. Rep.* **3**, 1134 (2013).
25. Viculis, L. M., Mack, J. J., Mayer, O. M., Hahn, H. T. & Kaner, R. B. Intercalation and exfoliation routes to graphite nanoplatelets. *J. Mater. Chem.* **15**, 974–978 (2005).
26. Park, S. J. & Ruoff, R. S. Chemical methods for the production of graphenes. *Nat. Nanotechnol.* **4**, 217–224 (2009).
27. Chen, D., Feng, H. B. & Li, J. H. Graphene oxide: preparation, functionalization, and electrochemical applications. *Chem. Rev.* **112**, 6156–6214 (2012).
28. Li, D., Müller, M. B., Gilje, S., Kaner, R. B. & Wallace, G. G. Processable aqueous dispersions of graphene nanosheets. *Nat. Nanotechnol.* **3**, 101–105 (2008).
29. Eda, G., Fanchini, G. & Chhowalla, M. Large-area ultrathin films of reduced graphene oxide as a transparent and flexible electronic material. *Nat. Nanotechnol.* **3**, 270–274 (2008).
30. Dreyer, D. R., Park, S. J., Bielawski, C. W. & Ruoff, R. S. The chemistry of graphene oxide. *Chem. Soc. Rev.* **39**, 228–240 (2010).
31. Guo, S. J. & Dong, S. J. Graphene nanosheet: synthesis, molecular engineering, thin film, hybrids, and energy and analytical applications. *Chem. Soc. Rev.* **40**, 2644–2672 (2011).
32. Becerril, H. A. *et al.* Evaluation of solution-processed reduced graphene oxide films as transparent conductors. *ACS Nano.* **2**, 463–470 (2008).
33. Shin, H. J. *et al.* Efficient reduction of graphite oxide by sodium borohydride and its effect on electrical conductance. *Adv. Funct. Mater.* **19**, 1987–1992 (2009).
34. Jeon, I. Y. *et al.* Edge-carboxylated graphene nanosheets via ball milling. *PNAS.* **109**, 5588–5593 (2012).
35. Hummers, Jr., W. S. & Offerman, R. E. Preparation of graphitic oxide. *J. Am. Chem. Soc.* **80**, 1339–1339 (1958).
36. Chandra, S. *Comprehensive inorganic chemistry*, 2nd ed., Deli, New Age International (P) Ltd, (2006).
37. Rodríguez-Pérez, L., Herranz, Ma. Á. & Martín, N. The chemistry of pristine graphene. *Chem. Commun.* **49**, 3721–3735 (2013).
38. Pan, S. Y. & Aksay, I. A. Factors controlling the size of graphene Oxide sheets produced via the graphite oxide route. *ACS Nano.* **5**, 4073–4083 (2011).
39. Chen, H. Q., Müller, M. B., Gilmore, K. J., Wallace, G. G. & Li, D. Mechanically strong, electrically conductive, and biocompatible graphene paper. *Adv. Mater.* **20**, 3557–3561 (2008).
40. Stankovich, S., Piner, R. D., Nguyen, S. T. B. & Rouff, R. S. Synthesis and exfoliation of isocyanate-treated graphene oxide nanoplatelets. *Carbon* **44**, 3342–3347 (2006).
41. Hontoria-Lucas, C., López-Peinado, A. J., López-González, J. D., Rojas-Cervantes, M. L. & Martín-Aranda, R. M. Study of oxygen-containing groups in series of graphite oxides: physical and chemical characterization. *Carbon* **33**, 1585–1592 (1995).
42. Kamimura, H. Graphite intercalation compounds. *Phys. Today.* **40**, 64–71 (1987).
43. Dikin, D. A. *et al.* Preparation and characterization of graphene oxide paper. *Nature* **448**, 457–460 (2007).
44. Ferrari, A. C. & Basko, D. M. Raman spectroscopy as a versatile tool for studying the properties of graphene . *Nat. Nanotechnol.* **8**, 235–246 (2013).
45. Stankovich, S. *et al.* Synthesis of graphene-based nanosheets via chemical reduction of exfoliated graphite oxide. *Carbon* **45**, 1558–1565 (2007)
46. Wang, J. Z., Manga, K. K., Bao, Q. L. & Loh, K. P. High-yield synthesis of few-layer graphene flakes through electrochemical expansion of graphite in propylene carbonate electrolyte. *J. Am. Chem. Soc.* **133**, 8888–8891 (2011).
47. Nair, R. R. *et al.* Fine structure constant defines visual transparency of graphene. *Science* **320**, 1308 (2008)
48. Ang, P. K., Wang, S., Bao, Q. L., Thong, J. T. L. & Loh, K. P. High-throughput synthesis of graphene by intercalation−exfoliation of graphite oxide and study of ionic screening in graphene transistor. *ACS Nano.* **3**, 3587–3594 (2009).
49. Matsuo, Y., Niwa, T. & Sugie, Y. Preparation and characterization of cationic surfactant-intercalated graphite oxide. *Carbon* **37**, 897–901 (1999).
50. Liu, Z. H., Wang, Z. M., Yang, X. J. & Ooi, K. Intercalation of organic ammonium ion into layered graphite oxide. *Langmuir* **18**, 4926–4932 (2002).
51. Lagaly, G. & Weiss, A. Zur van-der-Waals wechselwirkung in n-dodeclyammoium-schichtsilicaten. *Z Naturforsch.* **24B**, 1057–1058 (1969).
52. Tarascon, J. M. & Armand, M. Issues and challenges facing rechargeable lithium batteries. *Nature* **414**, 359–367 (2001).
53. Lee, S. W. *et al.* High-power lithium batteries from functionalized carbon-nanotube electrodes. *Nat. Nanotechnol.* **5**, 531–537 (2010).
54. Byon, H. R., Gallant, B. M., Lee, S. W. & Shao-Hon, Y. Role of oxygen functional groups in carbon nanotube/graphene freestanding electrode for high performance lithium batteries. *Adv. Func. Mater.* **23**, 1037–1045 (2013).
55. Kim, H. Y. *et al.* Scalable functionalized graphene nano-platelets as tunable cathodes for high-performance lithium rechargeable batteries. *Sci. Rep.* **3**, 1506 (2013).
56. Yoo, E. J. *et al.* Large reversible Li storage of graphene nanosheet families for use in rechargeable lithium ion batteries. *Nano Lett.* **8**, 2277–2281 (2008).


## Acknowledgements

We thank for the financial support from the National Natural Science Foundation of China (No. 51272155), the Foundation for SMC Excellent Young Teacher in Shanghai Jiao Tong University.

## Author contributions

L.W. designed the research. L.W., F.W. and D.S. prepared and characterized EOG and GO. C.H., X.L., J.W., J.Z., H.G., H.W., Y.W. and N.H. analyzed and interpreted the data. L.W., W.Y. and Y.Z. co-wrote the manuscript and supporting information.

## Additional information

**Supplementary information** accompanies this paper at http://www.nature.com/scientificreports

**Competing financial interests:** The authors declare no competing financial interests.

**How to cite this article:** Wei, L. *et al*. Spontaneous intercalation of long-chain alkyl ammonium into edge-selectively oxidized graphite to efficiently produce high-quality graphene. *Sci. Rep.* **3**, 2636; DOI:10.1038/srep02636 (2013).